Available online at www.sciencedirect.com
ScienceDirect
International Journal of Heat and Mass Transfer 50 (2007) 1176–1185
International Journal of HEAT and MASS TRANSFER
www.elsevier.com/locate/ijhmt

Fluid flow and heat transfer in an optical fiber coating process

Sang-Yeoun Yoo, Yogesh Jaluria *

Department of Mechanical and Aerospace Engineering, Rutgers, The State University of New Jersey, 98 Brett Road, Piscataway, NJ 08854-8058, United States

Received 1 June 2005; received in revised form 4 February 2006
Available online 11 January 2007

Abstract

The optical fiber coating process, using a die and applicator system, was numerically simulated. The coupled partial differential equations, governing the fluid flow and heat transfer, were solved on a transformed, non-uniform, staggered grid. A finite volume method, with conjugate heat transfer, boundary-fitted grid, and variable transport properties, was employed. The pressure was calculated using a SIMPLE-based algorithm. An isothermal case was first modeled, where the effect of the Reynolds number (*Re*) was studied for different geometries. Different coating fluids were considered. A conjugate boundary condition was employed at the fiber–fluid interface for the non-isothermal flow. A free surface boundary condition was used at the fiber entry into the coating fluid. The meniscus was prescribed on the basis of prior experimental work. Regardless of fiber speed, a circulating flow was observed in the applicator. High shear rates at the dynamic contact point suggest that air can be entrained with a fast moving fiber. It was also found that pressures at the coating fluid inlet did not play a major role, for typical fiber speeds, whereas the thermal conditions that affect the properties of the fluid, such as viscosity, made a significant impact on both the flow and the thermal field. This work could be used to determine the parameters that are critical for improving the quality of the coating, particularly its uniformity, and the production rate.

1. Introduction

An optical fiber drawn from a preform in a heated draw furnace typically goes through a cooling process [1], a coating process [2–6], and an ultraviolet(UV)-curing process [7]. In order to increase drawing speeds for the higher production rates, a quantitative knowledge of the coating process is critical. During the coating process, it has been found that air entrainment into the applicator may occur due to breakdown of the upper meniscus formed at the fiber entrance [5]. Therefore, the key parameters that play a major role in this phenomenon should be understood thoroughly to have a final product with desired quality, as indicated by coating uniformity, consistency, and adhesion. This study has been carried out to investigate the parameters that are involved in the coating process and to improve the coating quality by optimizing the design of the coating system.

Most of the earlier studies used simplified geometries of the applicator and the die for convenience in the analysis [3,5]. Chida et al. [3] reported that the fiber speed could reach 360 m/min with a UV-curable resin used for the coating material, and that the coating speed was constrained by the die when a thermally curable resin was used. A pressurized die was employed for their experiments. The final coating thickness was calculated from the mass flow rates measured at the die exit for their comparison with the theoretical values. They varied the pressure at the die entrance to control the coating thickness. Paek [5] summarized some of the important aspects involved in the coating process. He categorized coating materials into two types, one being organic materials, such as UV-curable materials and thermally curable materials. The other group includes inorganic materials, such as metallic coatings and carbon coatings. He indicated that the draw speed and the fiber strength were limited by the high shear rate at the fiber surface in the die.

Recently, a few attempts have been made to study the flow numerically [4,6,8]. Lyytikainen [4] used a commercial

* Corresponding author. Tel.: +1 732 445 3652; fax: +1 732 445 3124.
E-mail address: jaluria@jove.rutgers.edu (Y. Jaluria).

0017-9310/$ - see front matter © 2006 Elsevier Ltd. All rights reserved.
doi:10.1016/j.ijheatmasstransfer.2006.02.006

Nomenclature

c	specific heat
D	diameter
h	convection heat transfer coefficient
H	height
k	thermal conductivity
P	pressure
r	radial distance
T	temperature
u	radial velocity
v	axial velocity
z	axial distance

Greek symbols

α	thermal diffusivity
μ	dynamic viscosity
ρ	density
Φ	viscous dissipation

Subscripts

app	applicator
f	fiber
in	interface

software, the fluid dynamics analysis package (FIDAP), to analyze the coating fluid flow. A UV-curable acrylate was selected for the coating material. He also employed a conical-shaped design for the die and assumed the flow to be axisymmetric. His inputs for the simulation were the fiber and die wall temperatures, drawing speed, physical properties of the coating material, and the die geometry, which basically involved only the die entrance and exit diameters. He found that the maximum pressure occurred in the die near the sharp corner of the die entrance, and that this may trigger instability. A very high viscous heating was also observed in the die. He reported that altering the taper angle of the lower portion of the die did not significantly change the temperature, velocity, and pressure fields.

Dimitropoulos et al. [6] also used FIDAP to simulate the coating flows in the die. The die was similar to that of Lyytikainen [4], and the entire outer wall of the applicator was treated as an inlet at which the normal stress was specified. The viscosity of the coating material was taken as constant. Both menisci, at the fiber entrance dynamic contact point and at the die exit, were considered for the simulation. However, the dynamic contact angle and the slip coefficient were specified at the dynamic contact point to avoid a non-integrable singularity. The fiber speed ranged from 10 to 20 m/s, and the inlet normal stress was given as high as 1 MPa. They found that the increase in the inlet pressure for high fiber velocities resulted in a linear increase in the coating thickness with pressure. However, the physical variation in the thickness was extremely small. They also found that a change in the inlet pressure resulted in a dislocation of the dynamic contact point, as well as a change in the meniscus shape. As pointed out in the paper, their work was rather preliminary, since one of the most critical aspects, the thermal effects, were not considered.

The current study investigates an isothermal case first in order to determine how the flow behaves when a fast moving fiber passes through a coating fluid. Glycerin was selected for the coating material since a concurrent experimental study employed this fluid [9]. Its viscosity is based on the inlet temperature. When the thermal field was sought, a temperature-dependent viscosity was used, as shown in Fig. 1 [10]. Since the flow involves conjugate heat transfer at the fiber–fluid interface, where transport occurs between the fluid and the fiber, a coupled calculation for the two regions was carried out to solve for the flow and the thermal fields.

The geometric effects were also studied. Both the applicator and die geometries were varied, with all the other parameters fixed. For the die geometry, the effects of die entrance and exit diameters on the flow were studied separately. Due to high viscous dissipation in the die at high fiber speeds, this effect was included in the calculations. Isothermal or adiabatic wall conditions were applied at the die wall, as well as at the applicator outer wall. The mass flow rates at the die exit were calculated, these rates being directly related to the coating thickness. Other materials such as UV-curable acrylate, 80% glycerin, low density polyethylene (LDPE), and SAE-30 engine oil were also studied. The first one is of particular interest in practical coating processes.

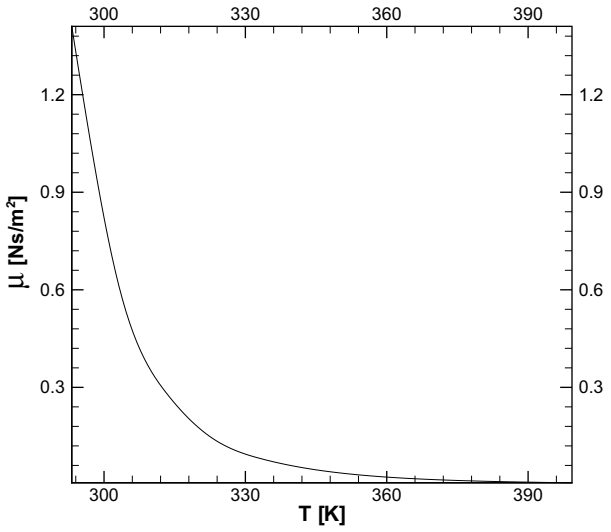

Fig. 1. Temperature-dependent viscosity used for glycerin [10].

2. Numerical analysis

2.1. Governing equations

The 2-D axisymmetric flow in an applicator and a die during the optical fiber coating process was simulated with a control volume method [11]. The cylindrical coordinate system fixed at the die exit is shown in Fig. 2. The fiber is moving at the center with a given speed [12]. The exact amount of the coating fluid coming out of the die exit is supplied to the applicator through the inlet, which is located circumferentially at the outer wall of the applicator. This is to ensure the mass balance during the calculations. Since the current study involves a highly non-uniform thermal field, the viscosity is treated as temperature dependent. The conservation equations for mass and momentum are [8]:

$$\frac{1}{r}\frac{\partial}{\partial r}(r\rho u)+\frac{\partial}{\partial z}(\rho v)=0 \tag{1}$$

$$\frac{1}{r}\frac{\partial}{\partial r}(r\rho u^2)+\frac{\partial}{\partial z}(\rho uv)=-\frac{\partial P}{\partial r}+\frac{1}{r}\frac{\partial}{\partial r}\left(r\mu\frac{\partial u}{\partial r}\right)+\frac{\partial}{\partial z}\left(\mu\frac{\partial u}{\partial z}\right)+\frac{1}{r}\frac{\partial}{\partial r}\left(r\mu\frac{\partial u}{\partial r}\right)+\frac{\partial}{\partial z}\left(\mu\frac{\partial v}{\partial r}\right)-2\mu\frac{u}{r^2} \tag{2}$$

$$\frac{1}{r}\frac{\partial}{\partial r}(r\rho uv)+\frac{\partial}{\partial z}(\rho v^2)=-\frac{\partial P}{\partial z}+\frac{1}{r}\frac{\partial}{\partial r}\left(r\mu\frac{\partial v}{\partial r}\right)+\frac{\partial}{\partial z}\left(\mu\frac{\partial v}{\partial z}\right)+\frac{1}{r}\frac{\partial}{\partial r}\left(r\mu\frac{\partial u}{\partial z}\right)+\frac{\partial}{\partial z}\left(\mu\frac{\partial v}{\partial z}\right) \tag{3}$$

The additional terms due to the temperature-dependent viscosity are the fourth and fifth terms on the right hand side of Eqs. (2) and (3), respectively. The energy equation for the fluid is

$$\frac{1}{r}\frac{\partial}{\partial r}(r\rho cuT)+\frac{\partial}{\partial z}(\rho cvT)=\frac{1}{r}\frac{\partial}{\partial r}\left(kr\frac{\partial T}{\partial r}\right)+\frac{\partial}{\partial z}\left(k\frac{\partial T}{\partial z}\right)+\mu\Phi \tag{4}$$

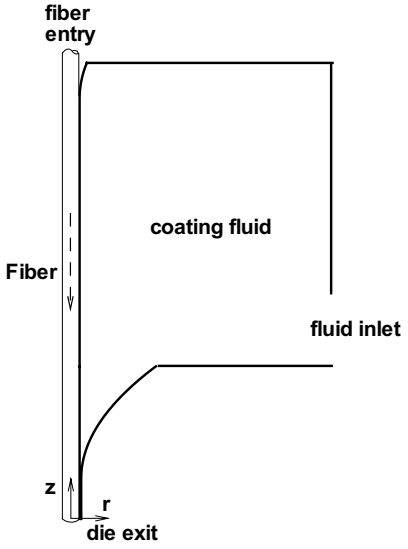

Fig. 2. Schematic diagram illustrating a typical coating applicator system.

where the viscous dissipation function is

$$\Phi=2\left[\left(\frac{\partial u}{\partial r}\right)^2+\left(\frac{u}{r}\right)^2+\left(\frac{\partial v}{\partial z}\right)^2\right]+\left(\frac{\partial u}{\partial z}+\frac{\partial v}{\partial r}\right)^2$$

For the fiber, the energy equation is

$$\rho_f c_f v_f\frac{\partial T}{\partial z}=\frac{2k_{in}}{r_f}\frac{\partial T}{\partial r} \tag{5}$$

Here, the fiber temperature is taken as lumped in the radial direction, since the Biot number, $Bi=\frac{hD_f}{k_f}$, is typically much less than 1.0. For example, for a fiber conductivity of 1.4 W/mK and for a typical fiber diameter of 125 μm, the equivalent value of the Bi, at a very high value of h, $h=5000\ \mathrm{W/m^2\,K}$, becomes 0.4464, which is still less than 1.0. The axial conduction in the fiber was neglected, this being very small compared to either the advection due to the moving fiber or the convection to the fluid [13]. For example, the Peclet number, $Pe=\frac{v_f D_f}{\alpha_f}$, becomes approximately 2027 for a typical fiber speed of 10 m/s. This implies that convection is dominant over the axial conduction in the fiber. The derivative on the right hand side of Eq. (5) is evaluated at the fiber surface where the higher-temperature fiber loses its energy by the convection to the cooler coating fluid, the two thermal conductivities being different. A harmonic mean of the two conductivities at the fiber–solid interface was used [14]. At the top surface, however, a free surface condition was applied. In addition, fully developed boundary conditions were employed at the die exit and no-slip conditions at the walls.

All the governing equations were transformed to obtain cylindrical computational domains [8]. Highly clustered grids were built near the walls as well as at the fiber. With increasing fiber speeds, shear rates in the die near the fiber become very high. The calculation was found to diverge, especially at high fiber speed, if the grids near the regions were not fine enough. Both axial and radial velocities were solved on staggered grids. A SIMPLE-based algorithm [14] was used, with contra-velocities chosen for the convection in the transformed domains. A second order upstream scheme [15] was used for the convective terms. This is to ensure diagonal dominance for the purpose of avoiding any numerical instability that may occur. The Thomas algorithm was used for solving the discretized equations, which were obtained with the alternating direction implicit (ADI) method [16]. The pressure equations were over-relaxed with a factor of 1.5 to enhance the convergence speed, whereas other variables such as velocities, temperature, and viscosity, were under-relaxed with that of 0.3 to obtain convergence of the non-linear governing equations [17]. The profile of upper meniscus that arises due to the entry of the fiber into the coating fluid, was prescribed for this study on the basis of earlier experimental results and a few test cases where the effects of its variation were not severe at fiber speeds considered in this study [18].

The effect of the geometries of the applicator and of the die was investigated in this study. As is shown in Table 1,

Table 1
Dimensions of the applicator and the die for various cases

Case	Fig. 8		Fig. 9	Fig. 10
	D_{app} [cm]	H_{app} [cm]	$D_{Die\,entrance}$ [μm]	$D_{Die\,exit}$ [μm]
1	1.6	1.42	3000	350
2	2.0	1.775	4000	450
3	2.4	2.13	5000	550
4	2.8	2.485	6000	650

the outer diameter (D) and the height (H) of the applicator were varied, with all the other geometric parameters fixed. For the die, however, the entrance die diameter was first varied. Then, the effect of the die exit diameter was studied.

2.2. Validation

The pressures at the fluid inlet to the applicator were calculated for various fiber speeds, employing the applicator system shown in Fig. 2. These pressures were extracted from the interior velocity fields and were compared with the experimental results [9,14]. During the experiments, the coating fluid, glycerin, was supplied using filtered compressed dry air in a pressurizing container and the flow rate was controlled by a two-valve system. A pressure transducer was used to measure the applicator pressure. As is shown in Fig. 3, they are in good agreement. The pressures measured during the experiments were varied at each fiber speed and their effects on the exit velocity profile of the coating material were monitored. Therefore, the pressures measured in the experiment are found to be comparable to the numerical values, since the mass flow rates match with each other.

The laminar flow in a pipe with a sudden contraction in its cross-sectional area was studied experimentally by Durst and Loy [19]. A laser-Doppler anemometer was employed for the measurements of the axial velocity profiles at various locations. Two separate pipes were mounted inside a square channel, which was filled with a fluid of the same refractive index as the glass material of the pipe wall. The axial velocity profiles at three locations in the pipe before contraction were compared with numerical predictions, as shown in Fig. 4. The Reynolds number (Re), based on the inlet diameter, was 196. The three axial locations, non-dimensionalized by the inlet diameter, were 0.209, 0.140, and 0.039. The coordinate system is fixed at the

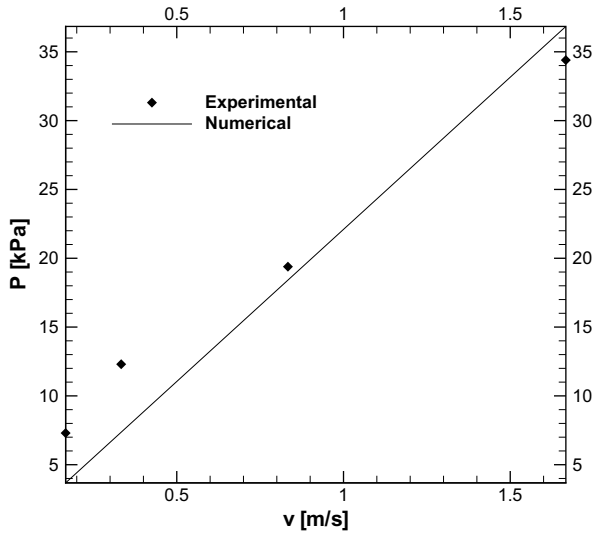

Fig. 3. Comparison of calculated inlet pressures with experimental data [9].

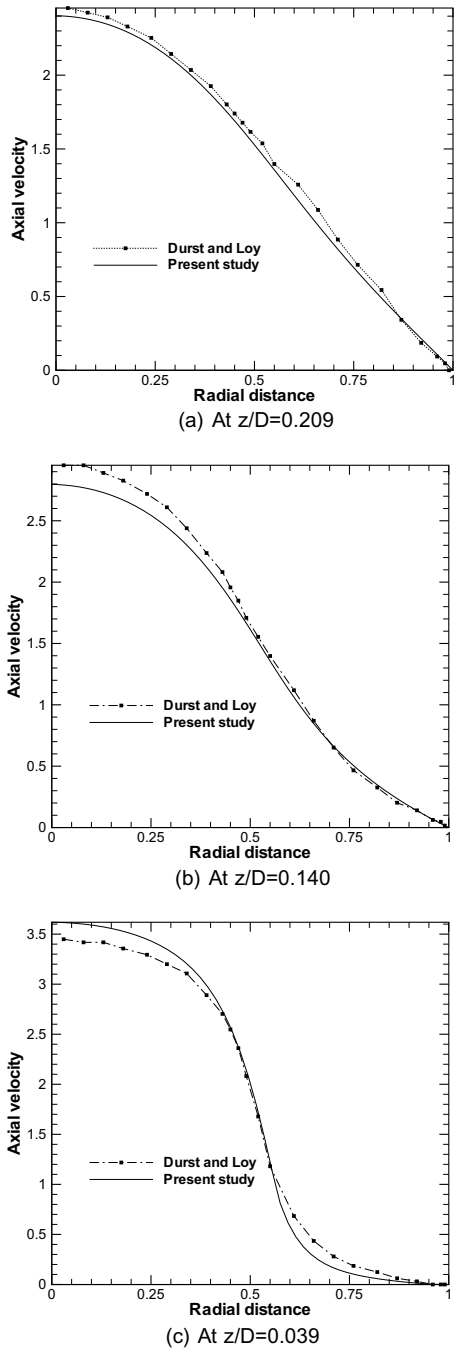

Fig. 4. Comparisons of axial velocity profiles at three different locations in a concentric tube with a sudden contraction, when $Re = 196$.

center of pipe where the contraction begins. The pipe entrance is located at $z/D = 32.5$, and the contraction is at $z/D = 0$. The two results were found to agree quite well. Fig. 4(a) shows that the fully developed velocity profile at the fluid entrance, $z/D = 32.5$, remains still intact at $z/D = 0.209$ which is near the start of the contraction. As the flow approaches the contracted region, it starts feeling the presence of the sudden area change and loses momentum near the wall, as seen in Fig. 4(b). The laminar flow becomes almost stagnant near the wall at the contraction and the flow at the center gains momentum, which resulted in the increased velocity profile at $z/D = 0.039$, as shown in Fig. 4(c).

3. Numerical results and discussion

3.1. Geometry effects

The isothermal case was investigated first to see how the flow field behaves under various operating conditions. The viscosity of the coating material, glycerin, was fixed at 1.1 N s/m^2 for $T = 296.6$ K, and the fiber speed was varied from 0.5 m/s to 18 m/s. The typical streamlines generated by the moving fiber are shown in Fig. 5. Regardless of fiber speed, a strong circulation was observed in the applicator. This circulation is largely responsible for removing thermal energy from the fiber and creating a non-uniform thermal field, as seen later from the non-isothermal case. The central portion of the circulation is dragged into the die by the fiber. Thus, the fluid coming into the die carries high momentum for large fiber speeds. This momentum, however, is balanced by the viscous force and the pressure built up in the die, mainly due to the continuous reduction in cross-sectional area of the die. Therefore, most of the fluid coming toward the die entrance is rejected by the high pressure and eventually rejoins the circulation in the applicator, as seen in Fig. 5.

The non-dimensional axial velocity profile at the die exit is shown in Fig. 6. This velocity is non-dimensionalized by the fiber speed. It was found that all the profiles vary almost linearly with the radial distance. However, it should be noted that they are calculated under isothermal conditions, with uniform fluid viscosity. Care should be taken when various thermal conditions are considered, since a non-isothermal thermal field can lead to large changes in the viscosity of the coating material. These effects are discussed later.

The shear rates along the fiber, for two fiber speeds, are shown in Fig. 7. It is seen that, at the dynamic contact point, very high shear rates arise and may allow air to enter the fluid zone, so that it may degrade the coating quality due to entrapped air bubbles. Near the die exit, where

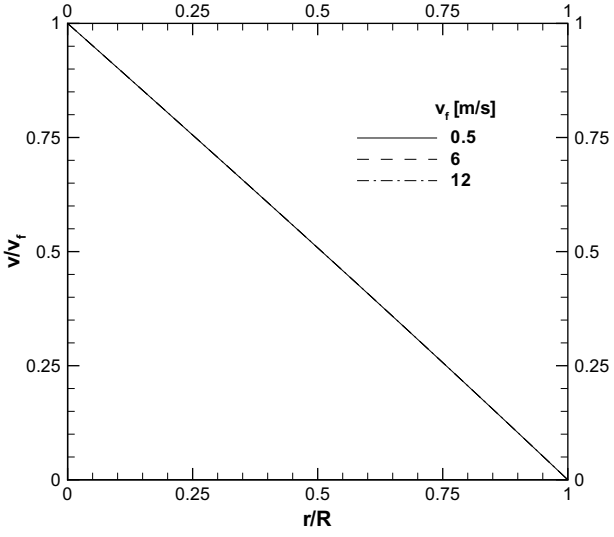

Fig. 6. Axial velocity profile for glycerin at the die exit, when isothermal condition is used with various fiber speeds.

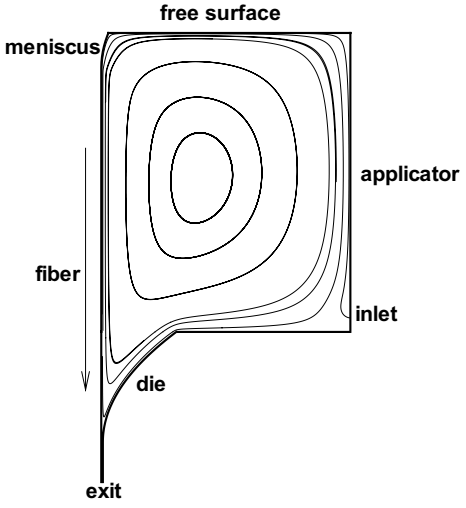

Fig. 5. Typical streamlines for glycerin, when isothermal condition is used with a fiber speed of 12 m/s.

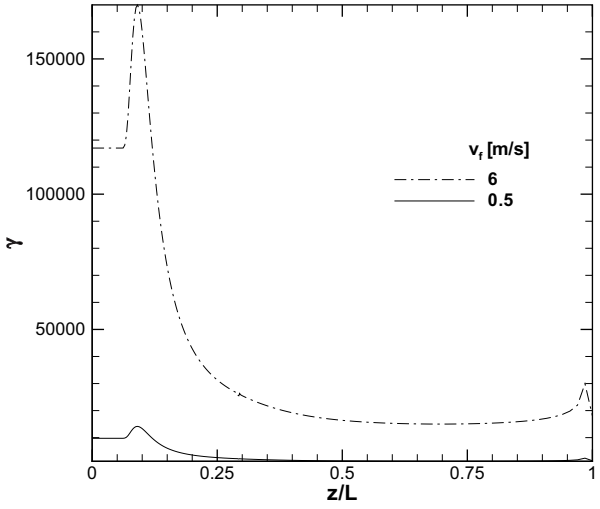

Fig. 7. Shear rates along the fiber for glycerin, when isothermal condition is used.

the straight duct starts, even higher shear rates were observed. This is partly due to the maximum pressures in the die and the circulation that exists there. Since viscous heating is not included, isothermal conditions yield lower temperatures and result in higher viscosities such that shear rates are higher. These high shear rates are known to damage the fiber surface and a proper heating is typically recommended to reduce the viscosity [5]. An approximate pulling tension was calculated by integrating the shear stress over the fiber surface by Paek [5]. Clearly, a quantitative knowledge of air entrainment, coating tension, and dynamic pressure in the die is very important for design and operation of the system.

Fig. 8 shows the effect of applicator geometry on the flow. The dimensions of the applicator for four different cases are shown in Table 1. Fig. 8(a) shows that the mass flow rate at the die exit varies linearly with the fiber speed and that the applicator geometry does not significantly affect the mass flow rate. The maximum pressure in the die also increases linearly with fiber speed and does not change substantially, as seen in Fig. 8(c). However, Fig. 8(b) shows that inlet pressures in the applicator, relative to the pressures at the dynamic contact point, changes with the size of the applicator, which suggested that more accurate calculations are required for the characterization of the free surface flow near the dynamic contact point.

Similar results were obtained for various die entrance diameters. Fig. 9(a) shows that the mass flow rate increases linearly with fiber speed and is not affected much by the die entrance diameter. As is obvious from Fig. 9(b), the diameter at the die entrance does not significantly affect the pressure at the dynamic contact point. However, a smaller die entrance allows slightly more mass into the die, resulting in higher pressures, as seen in Fig. 9(c).

The diameter of the die exit was also varied, as shown in Fig. 10. A bigger die exit leads to smaller resistance to the fluid coming out of the die, so that mass flow rates were higher and maximum pressures in the die were lower. However, the inlet pressures in the applicator, relative to the pressure at the dynamic contact point, were close to each other, regardless of the exit diameter. Thus, based on Figs. 9 and 10, it is seen that the die geometry does not significantly affect the flow in the applicator, in contrast to the flow in the die. This suggests that, as far as upper meniscus modeling is concerned, the shape or size of die can be quite flexible.

3.2. Thermal effects

The thermal conditions are found to be critical in this simulation, as seen in Figs. 11–13. Various thermal conditions were used for a fixed geometry, as seen in Table 2.

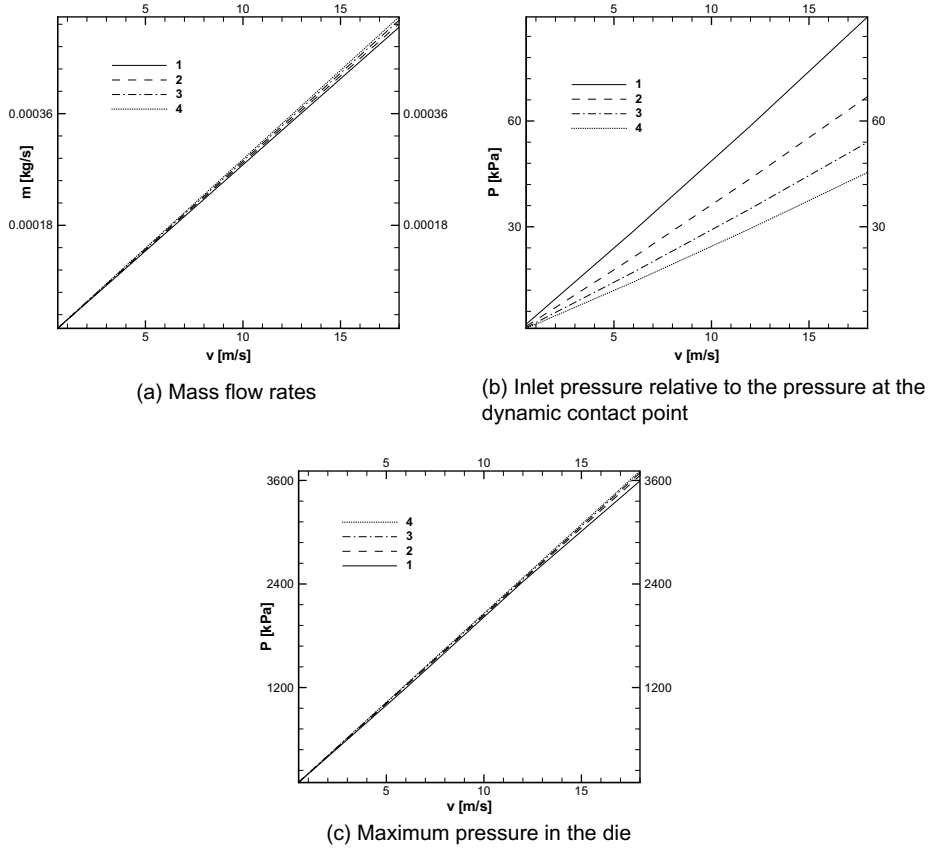

Fig. 8. Effects of applicator geometry for glycerin, when isothermal condition is used. The cases considered are from Table 1.

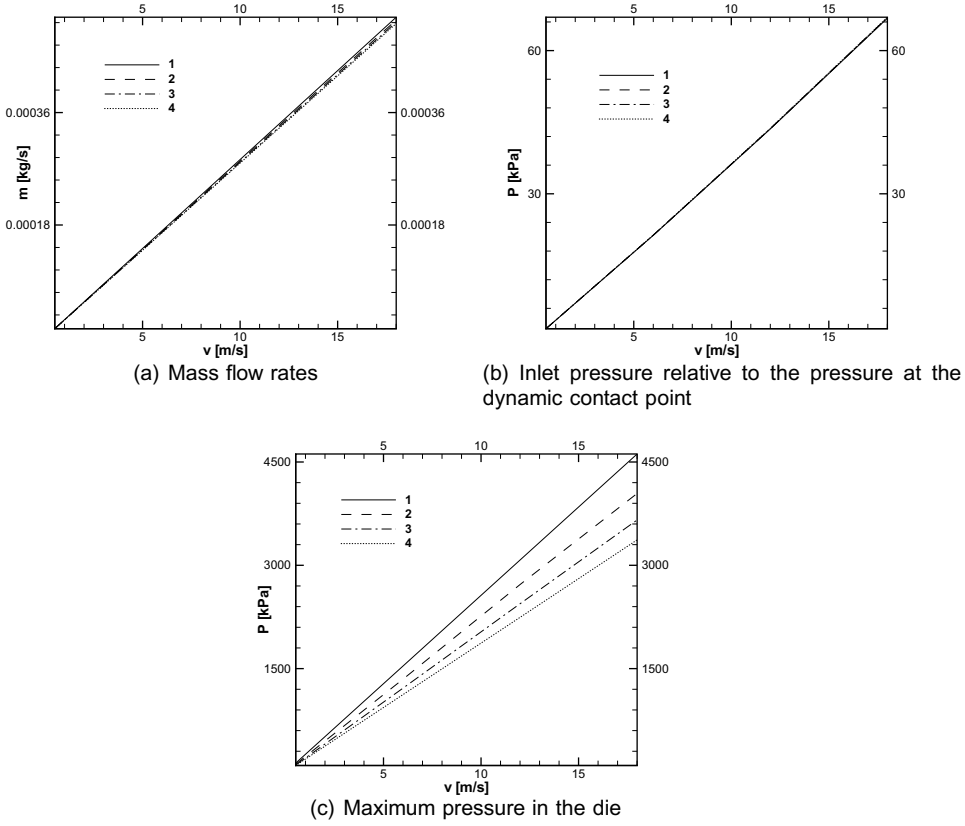

(a) Mass flow rates

(b) Inlet pressure relative to the pressure at the dynamic contact point

(c) Maximum pressure in the die

Fig. 9. Effects of die entrance diameter for glycerin, when isothermal condition is used. The cases considered are from Table 1.

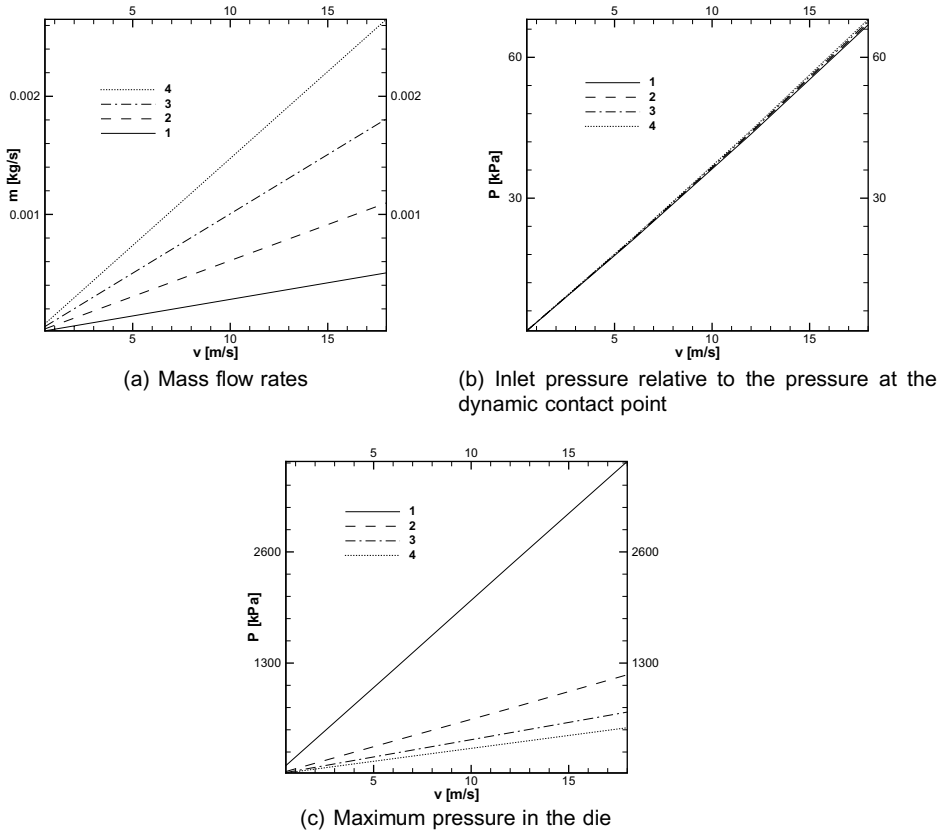

(a) Mass flow rates

(b) Inlet pressure relative to the pressure at the dynamic contact point

(c) Maximum pressure in the die

Fig. 10. Effects of die exit diameter for glycerin, when isothermal condition is used. The cases considered are from Table 1.

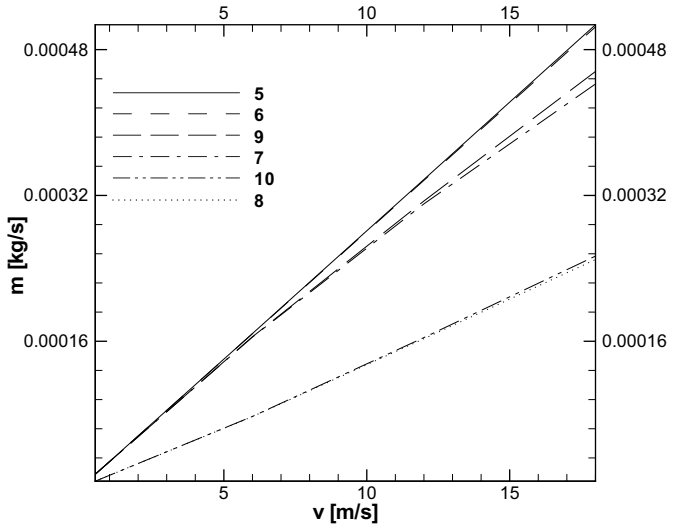

Fig. 11. Comparisons of mass flow rates at the die exit for different viscosities, which are referred to Table 2.

The viscostiy was taken as either constant or temperature-dependent. For the constant viscosity, the reference temperatures were based on the fluid inlet temperature or the average temperature of the fiber and the inlet. Adiabatic or isothermal conditions were applied to solid walls. Viscous heating was included for most cases, but two cases, 7 and 8, excluded it in order to study its overall effect.

As seen in Fig. 11, the mass flow rate at the die exit was found to depend on the thermal conditions in the domain. When the fluid viscosity was fixed, mass flow rates were found to be higher than for the temperature-dependent viscosity, and a reference temperature on which the viscosity was based was not important. Practically, the viscosity of the coating material in the applicator system is highly dependent on temperature, as shown in Fig. 1. Thus, the coating thickness based on the fixed viscosity may lead to erroneous results, which are found to be almost insensitive to a variation in the viscosity. When the fluid viscosity varies with temperature, wall conditions were found to be of critical importance. This is due to a highly non-uniform thermal field that is largely responsible for the flow behavior in the applicator and the die. Adiabatic conditions (cases 7 and 9) yield higher mass flow rates than the isothermal wall conditions (cases 8 and 10) did. The results become more apparent when the fiber speed is increased.

The temperatures along the fiber are seen in Fig. 12. The viscosities used were either taken as constant or temperature-dependent, and viscous dissipation was included or excluded. The fiber speed was fixed at 12 m/s and an adiabatic thermal condition was applied at the walls. The hotter fiber entering the applicator and die system loses its energy by the convection to the cooler fluid. Thus, the temperature decreases from the dynamic contact point to the die exit. It was found that temperature difference in the die is very high at higher fiber speeds for a constant viscosity, and that the fiber temperatures in the die start increasing. This indicates that a constant property approach to solve for the thermal field has to be considered with extreme caution and that incorporation of thermal effects into calculations is recommended in general.

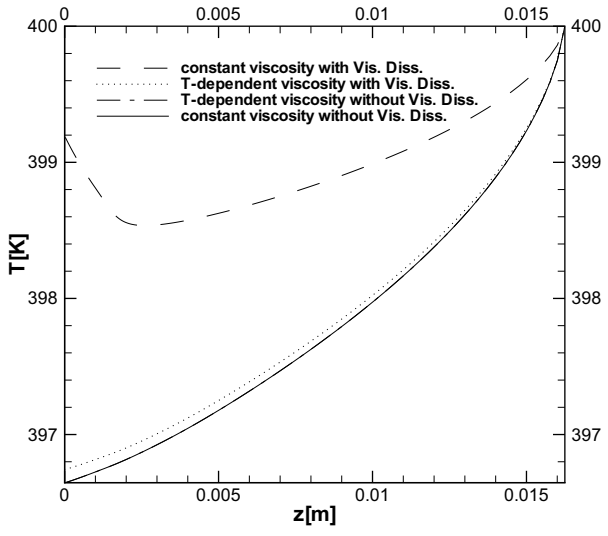

Fig. 12. Effects of viscosity variation and viscous dissipation on the fiber temperature for glycerin when adiabatic boundary conditions are used with a fiber speed of 12 m/s.

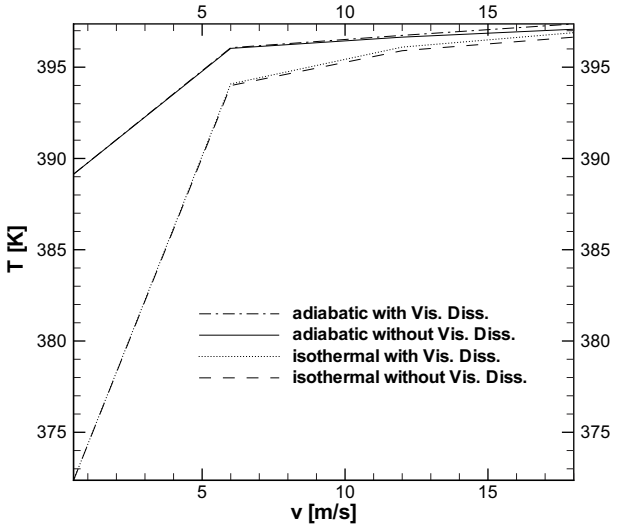

Fig. 13. Effects of the boundary condition on the fiber temperature at the die exit when the temperature-dependent viscosity is used for glycerin.

Table 2
Thermal conditions used include isothermal walls whose temperatures are as same as the ambient at 300 K

Case	Condition
5	$\mu = 0.0399$ at $T = 348.3$ K, and isothermal walls
6	$\mu = 1.1000$ at $T = 296.6$ K, and isothermal walls
7	$\mu = \mu(T)$, adiabatic walls, and no viscous heating
8	$\mu = \mu(T)$, isothermal walls, and no viscous heating
9	$\mu = \mu(T)$, and adiabatic walls
10	$\mu = \mu(T)$, and isothermal walls

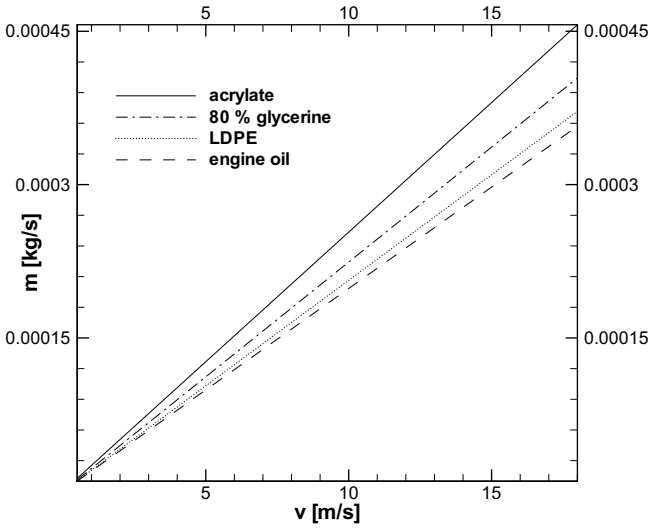

Fig. 14. Mass flow rates for various materials over a range of fiber speed, when isothermal condition is used.

Table 3
Material properties used

Property	Acrylate	80% glycerin	LDPE	Engine oil
Density [kg/m^3]	1130	997.5	920	884.1
Viscosity [N s/m^3]	17.35	0.0415	2000	0.486

The fiber temperature at the die exit is calculated and shown in Fig. 13. The temperatures at the exit were higher for adiabatic walls, irrespective of the presence of viscous dissipation, as long as temperature-dependent viscosities are used. This makes sense since the energy taken away from the fiber by the fluid is stored within the fluid for the case of adiabatic walls, so that less energy transfer occurs in the die. However, when the isothermal wall boundary condition is used, the fluid carrying the energy from the fiber loses most of the energy to the cooler die wall. One trend, that is common to both adiabatic and isothermal boundary conditions, is that the fiber temperature at the exit increases with the fiber speed.

Other coating materials were also investigated. Fig. 14 shows four materials used in the calculations and Table 3 has the properties used. All of them were considered under isothermal conditions. Acrylate has the highest mass flow rate at the die exit, whereas SAE 30 engine oil has the smallest. The mass flow rates increase linearly with the fiber speed. As was the case for glycerin where the viscosity is fixed at a reference temperature, there is no correlation between the viscosity of a material and the corresponding mass flow rate at the die exit. However, this should be studied further in detail because, as discussed earlier, the results from an isothermal study can be misleading.

4. Conclusions

In order to predict which parameters are critical for determining the quality of the coating, particularly its uniformity, and the production rate, various numerical results have been presented. Glycerin is first used for the coating material, but UV-curable materials are of greater interest in practical coating processes. Regardless of fiber speed, a strong circulation was observed in the applicator. This strong circulation is largely responsible for removing thermal energy from the fiber and creating a non-uniform thermal field. The axial velocity profiles at the die exit varied almost linearly with the radial distance for the isothermal case. Very high shear rates were observed both at the dynamic contact point and in the die, and these increased with the fiber speed. The effect of applicator geometry on the flow was found to be small. However, it did affect the pressure near the dynamic contact point, suggesting that more accurate calculations are necessary in this region. A change in die entrance diameter affected the maximum pressures in the die. However, when the die exit diameter was varied, both the mass flow rate and the maximum pressure were changed, indicating that great care should be taken in die design.

On the contrary, the thermal effects on the flow were found to be very significant. A noticeable difference in the flow fields was obtained by the choice of either constant viscosity or a temperature-dependent viscosity. The thermal boundary conditions along the boundary, such as constant temperature or adiabatic walls, turned out to be very important. Due to the high viscous heating in the die at higher fiber speeds, the effect of viscous dissipation must be included in the analysis. Variable fluid properties must also be considered.

The main purpose of the current work was to determine the critical effects involved in the optical fiber coating process by studying the coating flow and heat transfer. The effects of geometry, as well as the thermal effects, were investigated. The results presented in this study, therefore, can be used as a framework upon which an optimization of the coating applicator and die can be built, so that coating characteristics, such as uniformity, can be improved.

Acknowledgements

The authors gratefully acknowledge the support by National Science Foundation, under grant no. CTS-0119356, for this work and the discussions with Prof. Polymeropoulos on this problem.

References

[1] U. Paek, C. Schroeder, Forced convective cooling of optical fibers in high-speed coating, J. Appl. Phys. 50 (10) (1979) 6144–6148.
[2] N. Akasaka, T. Hattori, T. Nonaka, K. Oishi, Y. Matsuda, Design of optical fiber coating, in: Australian Conference on Optical Fiber Technology, 1994, pp. 375–378.
[3] K. Chida, S. Sakaguchi, M. Wagatsuma, T. Kimura, High-speed coating of optical fibers with thermally curable silicone resin using a pressurized die, Electron. Lett. 18 (16) (1982) 713–715.
[4] K. Lyytikainen, Numerical simulation of the optical fiber coating process, Wire Technol. Int. 26 (2) (1998) 132–134.

[5] U. Paek, Free drawing and polymer coating of silica glass optical fibers, J. Heat Transfer 121 (1999) 774–788.
[6] C. Dimitropoulos, S. Chippada, E. Grald, J. Kulkarni, CFD simulation of optical fiber coating flows, in: Proc. 49th Int. Wire and Cable Sym., NJ, 2000, pp. 89–96.
[7] U. Paek, C. Schroeder, Calculation of photopolymerization energy required for optical fiber coating, Appl. Opt. 20 (7) (1981) 1230–1233.
[8] K. Rattan, Y. Jaluria, Simulation of the flow in a coating applicator for optical fiber manufacture, Comput. Mech. 31 (5) (2003) 428–436.
[9] S. Ravinutala, C. Polymeropoulos, Entrance meniscus in a pressurized optical fiber coating applicator, Exp. Therm. Fluid Sci. 26 (2002) 573–580.
[10] C. Miner, N. Dalton, Glycerol, no. 117, American Chemical Society Monograph Series, 1952.
[11] D. Pan, C. Chang, Upwind finite-volume method for natural and forced convection, Numer. Heat Transfer Part B 25 (2) (1999) 177–191.
[12] X. Cheng, Y. Jaluria, Effect of furnace thermal configuration on optical fiber heating and drawing, Numer. Heat Transfer Part A 48 (6) (2005) 507–528.
[13] F. Incropera, D. Dewitt, Introduction to Heat Transfer, third ed., John Wiley Sons, 1996.
[14] S. Patankar, Numerical Heat Transfer and Fluid Flow, Taylor and Francis, 1980.
[15] S. Thakur, W. Shyy, Some implementational issues of convection schemes for finite-volume formulations, Numer. Heat Transfer Part B 24 (1993) 31–55.
[16] K. Hoffmann, S. Chiang, Computational Fluid Dynamics, fourth ed., Engineering Education System, Kansas, 2000.
[17] Y. Jaluria, Computer Methods for Engineering, Prentice-Hall, Englewood Cliffs, NJ, 1988.
[18] A. Abraham C. Polymeropoulos, Dynamic menisci on moving fibers, in: Proc. 48th Int. Wire and Cable Sym., NJ, 1999, pp. 520–524.
[19] F. Durst, T. Loy, Investigation of laminar flow in a pipe with sudden contraction of cross sectional area, Comput. Fluids 13 (1) (1985) 15–36.